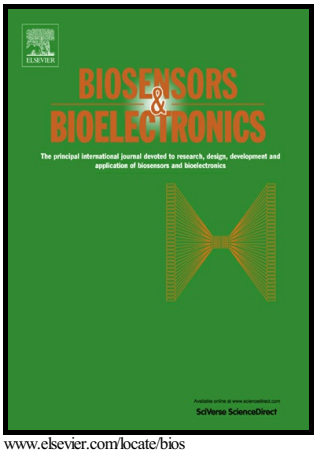

www.elsevier.com/locate/bios

CeO_2 nanocrystallines ensemble-on-nitrogen-doped graphene nanocomposites: One-pot, rapid synthesis and excellent electrocatalytic activity for enzymatic biosensing

Xiaojiao Du, Ding Jiang, Saibo Chen, Liming Dai, Lei Zhou, Nan Hao, Tianyou You, Hanping Mao, Kun Wang

PII: S0956-5663(15)30607-2
DOI: http://dx.doi.org/10.1016/j.bios.2015.11.054
Reference: BIOS8184

To appear in: *Biosensors and Bioelectronic*

Received date: 22 October 2015
Revised date: 10 November 2015
Accepted date: 17 November 2015

Cite this article as: Xiaojiao Du, Ding Jiang, Saibo Chen, Liming Dai, Lei Zhou Nan Hao, Tianyou You, Hanping Mao and Kun Wang, CeO $_2$ **nanocrystalline ensemble-on-nitrogen-doped graphene nanocomposites: One-pot, rapi synthesis and excellent electrocatalytic activity for enzymatic biosensing** *Biosensors and Bioelectronic,* http://dx.doi.org/10.1016/j.bios.2015.11.054

CeO_2 nanocrystallines ensemble-on-nitrogen-doped graphene nanocomposites: one-pot, rapid synthesis and excellent electrocatalytic activity for enzymatic biosensing

Xiaojiao Du,‡[a] Ding Jiang,‡[b] Saibo Chen,[a] Liming Dai,[a] Lei Zhou,[a] Nan Hao[a] Tianyou You,[a] Hanping Mao[a] and Kun Wang*[a]

[a]Key Laboratory of Modern Agriculture Equipment and Technology, School of Chemistry and Chemical Engineering, Jiangsu University, Zhenjiang, 212013, P.R. China.

[b]School of Food and Biological Engineering, Jiangsu University, Zhenjiang, 212013, P.R. China.

‡ These authors contributed equally to this work.

Abstract:

Ceria nanomaterials for heterogeneous catalysis have attracted much attention due to their excellent properties and have been extensively applied in recent years. But the poor electron conductivity and the aggregation behavior severely affect their electrocatalytic performances. In this paper, we prepared a novel catalyst based on CeO_2 nanocrystallines (CeO_2 NCs) ensemble-on-nitrogen-doped graphene (CeO_2-NG) nanocomposites through a one-step heat-treatment without the need of the precursor. The results confirmed that the high dispersion of CeO_2 NCs with the uniform size distribution of about 5 nm on the surface of nitrogen-doped graphene (NG) sheets could be easily obtained via the one-step procedure and the resultant CeO_2-NG

* Corresponding author. Tel.: +86 511 88791800; fax: +86 511 88791708.
E-mail address: wangkun@ujs.edu.cn

nanocomposites were an excellent electrode material possessing outstanding electrochemical features for electron transfer. Luminol, an important electroactive substance, was further chosen to inspect the electrocatalytic properties of the as-prepared CeO_2-NG nanocomposites. The studies showed that the presence of the NG in CeO_2-NG nanocomposites could facilitate the electrochemical redox process of luminol. Compared with pristine CeO_2 NCs, the synthesized CeO_2-NG nanocomposites can enhance the electrochemiluminescence (ECL) intensity by 3.3-fold and decrease the onset ECL potential for about 72 mV in the neutral condition. Employing above superiority, selecting cholesterol oxidase (ChOx) as the model oxidase, a facile ECL method for cholesterol detection with the CeO_2-NG nanocomposites as the matrix to immobilize enzyme ChOx was developed. The results demonstrated CeO_2-NG nanocomposites exhibited excellent performances in terms of sensitivity and catalytic activities, indicating that NG-based nanomaterials have great promise in electrocatalytic and enzymatic biosensing fields.

Keywords: Nitrogen-doped graphene; CeO_2 nanocrystallines; Biosensor; Enzyme

1. Introduction

Semiconductor and metal oxide nanocrystals have been widely applied in nanoelectrochemistry, especially as catalysts in various catalytic reactions and become one of the most fascinating topics due to unique properties such as electronic, optical, and catalytic properties (Bai et al., 2015; Guo et al., 2010; Liu et al. 2014). Although the above-mentioned nanomaterials show a brilliant prospect, they are faced with one or several challenges hindering their practical applications: (1) nanocrystals are not stable and easy to aggregate because of their large specific surface area and high surface activity, lowering their catalytic activity (Jin et al., 2015; Jiang et al., 2015a); (2) metal oxide nanocrystals with low conductivity influence the charge transfer rate of the redox reaction in an electrochemical process (Jiang et al., 2012); (3) conventional preparation approaches for semiconductor nanocrystals mostly utilize multistep chemical methods wherein various strains of agents are employed, which makes it time-consuming and high-cost (Shah et al., 2012). Thereby, design and production of catalytic materials with high activity, stability, conductivity and a facile synthetic route is always the ultimate goal of catalyst manufacturers (Nørskov et al., 2009; Schwarz et al., 1995).

Nanostructure ceria (CeO_2) is an ideal candidate for heterogeneous catalysis because it can provide abundant active planes or oxygen vacancies, which are favorable for the catalytic activity (Du et al., 2012; Zhang et al., 2010). Among various systems, photocatalysis and electrocatalysis are two classes of reactions in which charge carriers play an important role (Bai et al., 2015). Like the conventional

nanocrystals, the as-prepared CeO_2 nanocrystallines (CeO_2 NCs) usually tend to form aggregates leading to a lower catalytic activity despite the high catalytic activity of NCs (Jiang et al., 2012). Particularly, the poor conductivity of CeO_2 NCs hindered their further applications in electrocatalytic fields (Chu et al., 2014). Moreover, the tedious synthetic process also restricted their extensive applications. In the last few years, it is one of the hot trends to incorporate the cerium with noble-metal Pt or Au (Chen et al., 2015; Liao et al., 2008; Manorama et al., 2003), and carbon-based nanomaterials for a large variety of applications (Su et al., 2013; Wang et al., 2012b; Xu et al., 2014). For instance, Liao et al. found that incorporation of Pt nanocrystals on CeO_2 could significantly increase the charge transfer rate between the Pt and CeO_2 (Liao et al., 2008). Although the performances of Ce-based materials have been improved in previous investigations, the expensive noble-metals and complicated steps are unfavorable. Therefore, exploring appropriate supporting substrates to anchor CeO_2 NCs is expected to enhance the dispersion, conductivity and promote the catalytic activity from CeO_2 NCs.

Nitrogen-doped graphene (NG), as a kind of nitrogen atoms doped into graphene carbon lattice, can serve as a high-performance support because of its ideal two-dimensional (2D) structure, huge specific surface area, and excellent electrical conductivity and has been intensively investigated as an electrode material for various fields (Chu et al., 2014; Rao et al., 2009; Wang et al., 2012a). The latest studies have demonstrated that the nitrogen functionality of the supporting substrates not only further facilitates the electron-transfer on the support–metal interface to enhance the

catalyst activity, but also promotes the dispersion of nanoparticles (Chu et al., 2014). In our past research, copper nanoparticles decorated NG (Cu–NG) were prepared using NG as a novel substrate material, showing enhanced electrocatalytic activity to glucose oxidation (Jiang et al., 2014). Thus, it is necessary to integrate CeO_2 NCs with NG, while there are few papers focused on the investigation into the synthetic method of CeO_2 NCs coupled with NG.

Herein, we reported the synthesis of CeO_2 NCs on the ensemble-on-NG graphene (CeO_2-NG) nanocomposites via a one-pot heat-treatment method without need of the precursor. With luminol as an important electroactive substance, the synthesized CeO_2-NG nanocomposites showed higher catalytic activity versus the reaction of luminol-H_2O_2 than the pristine CeO_2 NCs. As a result, CeO_2-NG nanocomposites modified electrode generated strong ECL emission in the neutral luminol solution. Luminol has become one of the most popular coreactant electrochemiluminescence (ECL) reagents due to its availability and low cost (Ballesta-Claver et al., 2012; Zhang et al., 2014). Based on above facts, selecting cholesterol oxidase (ChOx) as the model oxidase, we developed a facile ECL method for cholesterol detection with the CeO_2-NG nanocomposites as the matrix for immobilizing enzyme ChOx. The catalytic activity of CeO_2-NG nanocomposites for luminol ECL was investigated in detail. The CeO_2-NG nanocomposites exhibited excellent performances in terms of sensitivity and catalytic activities, implying that NG-based materials have great promises in electrocatalytic and enzymatic biosensing applications.

2. Experimental

2.1. Reagents and chemicals

Graphite was purchased from Qingdao Tianhe Graphite Co., Ltd. Ammonium cerium nitrate ($(NH_4)_2Ce(NO_3)_6$) was purchased from Sinopharm Chemical Reagent Co. Ltd. The glycine (Gly) was purchased from Sinopharm Chemical Reagent Co., Ltd. Cholesterol (≥99% purity), cholesterol oxidase (EC 1.1.3.6, ≥50 units/mg), Triton X-100 and luminol (98%) were purchased from Sigma Chemical Co. (St. Louis, Mo, USA). Graphene oxide (GO) was prepared using modified Hummers method from graphite powders (Gilje et al., 2007). The stock solution was prepared by dissolving cholesterol in the mixture of 2-propanol and Triton X-100 and then diluted it only with Triton X-100 solution for preparing standard solutions. Phosphate buffer solution (PBS) was prepared by mixing standard stock solutions of NaH_2PO_4 and Na_2HPO_4, and adjusting the pH value with 0.1 M H_3PO_4 or NaOH. All of the other chemical reagents used in our experiments are of analytical grade, and used without further purification. Double-distilled water was used throughout the work.

2.2. Apparatus

The transmission electron microscope (TEM) images and high-resolution transmission electron microscopy (HRTEM) images were performed by using a JEOL JSM-6700 transmission electron microscope (Tokyo, Japan). X-ray diffraction (XRD) and Raman spectra were carried out on an X'Pert X-ray diffraction spectrometer (Philips, USA) and an RM 2000 microscopic confocal Raman spectrometer, respectively. X-ray photoelectron spectroscopy (XPS) was performed on a Thermo

VG Scientific ESCALAB 250 spectrometer with an Mg Kα radiator. The ECL emission was monitored with a model MPI-A electrochemiluminescence analyzer (Xi'an Remex Analysis Instrument Co. Ltd. Xi'an, China) with 800 V photomultiplier tube voltage. Electrochemical impedance spectroscopy (EIS) was performed in a 0.1 M KCl solution containing 5 mM $Fe(CN)_6^{3-/4-}$ with a frequency range from 0.01 Hz to 10 kHz at 0.23 V, and the amplitude of the applied sine wave potential in each case was 5 mV. Cyclic voltammetry (CV) experiments were performed on a CHI-660B electrochemical workstation (Chenhua Instruments Co., Shanghai, China). The conventional three-electrode system was employed with a modified glassy carbon electrode (GCE, 3 mm) as the working electrode, a Pt wire as the counter electrode, and a Ag/AgCl (saturated with KCl) as the reference electrode.

2.3. Preparation of CeO_2-NG nanocomposites

CeO_2-NG nanocomposites were synthesized by one-step heat-treatment (Scheme 1). Briefly, 5 mg of GO, 30 mg of glycine (Gly) and 60 mg of $(NH_4)_2Ce(NO_3)_6$ were dispersed in 5 mL of double-distilled water through sonication for several hours to give a homogeneous solution and then poured into an alumina crucible. Under the argon atmosphere, the temperature of the mixture was gradually raised to 500 ^oC and maintained for 2 h. Finally, the product could be directly collected from the alumina crucible. Similarly, the pristine CeO_2 NCs and CeO_2 NCs-graphene nanocomposites (CeO_2-GR) nanocomposites were synthesized except for the addition of GO or Gly, respectively.

2.4 Biosensor preparation

First, the GCE was polished with 0.3 and 0.05 μm alumina slurry repeatedly, followed by ultrasonic treatment with water and ethanol successively for 3 min and dried in air. Next, 6 μL CeO_2-NG suspension was dropped onto the pretreated GCE surface and dried at regulating temperature and then 6 μL chitosan solution (CHIT) was coated on the CeO_2-NG modified GCE (denoted as CHIT/CeO_2-NG/GCE). Subsequently, 6 μL ChOx solution was cast onto the electrode to obtain the biosensor ChOx/CHIT/CeO_2-NG/GCE. For comparison, ChOx/CHIT/CeO_2-GR/GCE and CHIT/CeO_2/GCE were prepared similarly. The biosensors were stored at 4 ^{o}C when not in use.

3. Results and discussion

3.1. Morphology and composition

The TEM image of CeO_2-NG nanocomposites was displayed in Fig. 1A. It was clear that the two-dimensional NG sheet was well decorated by a large quantity of CeO_2 NCs and the both outlines of CeO_2 NCs and NG could be clearly observed. It is noticeable that CeO_2 NCs were well-dispersed on NG sheets with the average size of CeO_2 NCs of ca. 5 nm, while the pristine CeO_2 NCs easily tended to agglomerate (Fig. S1A and the CeO_2-GR nanocomposites exhibited similar morphology with CeO_2-NG nanocomposites (Fig. S1B), indicating graphene and NG sheets could act as an excellent support for CeO_2 NCs. The HRTEM image in Fig. 1B presented the clear (111), (200) and (220) lattice fringes of cubic CeO_2 with the interplanar spacing of 0.32, 0.27, and 0.19 nm, respectively (Yang et al., 2013). To know the crystalline structure of the obtained samples, the as-synthesized pristine CeO_2 NCs, CeO_2-GR

and CeO_2-NG nanocomposites were characterized by XRD measurements. From Fig. 1C, the as-synthesized pristine CeO_2 NCs, CeO_2-GR and CeO_2-NG nanocomposites all exhibited a typical cubic phase of ceria (α= 5.411 Å, JCPDS Card no. 34−0394), which suggested that the crystal structure of CeO_2 NCs were not affected by GR or NG component (Jiang et al., 2012; Yang et al., 2013). As we all know, Raman spectroscopy is a powerful and widely used tool to characterize the structural properties of graphene-based materials, such as disorder and defect structures (Ji et al., 2014). Fig. 1D showed the recorded Raman spectra of NG, pristine CeO_2 NCs and CeO_2-NG nanocomposites. From the spectra, the Raman spectrum of NG displayed two prominent peaks at 1346 and 1577 cm^{-1}, corresponding to the well-documented D and G bands, respectively (Jiang et al., 2015b). Moreover, as for the CeO_2-NG nanocomposites, the D band shifted from 1346 cm^{-1} to 1356 cm^{-1} and the G band shifted from 1577 cm^{-1} to 1597 cm^{-1} compared with NG, suggesting that there is effective charge transfer between the graphene sheets and pristine CeO_2 NCs in the CeO_2-NG nanocomposites (Jiang et al., 2015a; Jha et al., 2014). Besides, the peaks at 453 cm^{-1} in the pristine CeO_2 NCs and CeO_2-NG nanocomposites can be assigned to the F_{2g} vibration mode of the anchored CeO_2 NCs and the oxygen vacancies in the CeO_2 (Jiang et al., 2012; Ji et al., 2014). These results confirmed that the existence of NG and CeO_2 NCs in the CeO_2-NG nanocomposites.

Furthermore, the compositional analysis of CeO_2-NG nanocomposites was performed using XPS. The full range scan XPS spectrum of CeO_2-NG confirmed the three elements (C, N and Ce) in the nanocomposites (Fig. 2A). In the XPS spectrum

of N 1s for the CeO_2-NG nanocomposites (Fig. 2B), the two well-resolved peaks located at 398.1 and 400.2 eV ascribed to the pyridine nitrogen and pyrrolic nitrogen atoms, whereas four peaks centered at 284.8, 285.9, 287.2, and 289.1 eV of the deconvoluted C 1s XPS spectrum (Fig. 2D) represented sp^2-sp^2 C, N-sp^2 C, N-sp^3 C, and C−O type bonds, respectively (Jiang et al., 2015a). The deconvoluted XPS spectra of the Ce 3d were depicted in Fig. 2C. The XPS spectra of Ce 3d of the CeO_2-NG can be assigned to $3d_{5/2}$ states (labelled V) and $3d_{3/2}$ spin-orbit states (labelled U) (Srivastava et al., 2013; Yang et al., 2013). The existence of a shoulder peak at 885.1 eV (V_2) and a tiny peak at about 904.8 eV (U_2) in the Ce 3d spectrum, corresponding to the Ce^{3+} state which may be ascribed to CeO_2 NCs interacted with the graphene nanosheet, a certain amount of Ce^{4+} turned into Ce^{3+} and some oxygen vacancies might be produced (Srivastava et al., 2013; Yang et al., 2013). The oxygen vacancies served as electron traps and increased the amount of absorbed oxygen in the sensing and thus promote the catalytic activity of CeO_2 NCs (Yang et al., 2013). Therefore, we could concluded that the component of CeO_2 NCs on the nitrogen doping graphene was realized in a facile step by our method.

As illustrated in Scheme 1, CeO_2-NG nanocomposites were synthesized via one-pot heat-treatment method. Equation 1 described a stoichiometric reaction for the present synthesis of CeO_2 NCs system (Mokkelbost et al., 2004).

$$9(NH_4)_2Ce(NO_3)_6 + 14\ NH_2CH_2COOH\ (Gly) \rightarrow 9CeO_2(s) + 4\ ½\ N_2(g) + 28\ CO_2(g) + 18NH_3(g) + 44H_2O\ (g) \quad (1)$$

In addition, it could be confirmed that the Gly acted as a source for nitrogen doping,

because there was no obvious nitrogen content observed in the controlled experiment without addition of Gly. Furthermore, Gly was exploited as the fuel to reduce NO_3^-, resulting in the decomposition for the mixture of Gly-nitrate (Jiang et al., 2015a). The decomposition products can promote the reduction of oxygen-containing functional groups on the surface of GO (Mayavan et al., 2012). As a result, well-dispersed CeO_2 NCs can be loaded on NG sheets.

3.2. Detection Principle of the Cholesterol Biosensor

As depicted in Scheme 1, the principle of the biosensor in the detection of cholesterol occurred as the following (Hong et al., 2013; Zhang et al., 2012):

$$\text{Cholesterol} + O_2 \xrightarrow{\text{ChOx}} \text{Cholest-4-en-3-one} + H_2O_2 \quad (2)$$

$$H_2O_2 + \text{luminol} \xrightarrow{CeO_2} \text{aminophthalate} + h\nu \quad (3)$$

Chemical reaction happened between cholesterol and oxygen in the presence of ChOx, and H_2O_2 was one of the products (Equation 2) (Hong et al., 2013;). Based on the previous reports in the study for the luminol-H_2O_2 ECL system, it was proposed that all sorts of reactive oxygen species (ROS) were generated from H_2O_2, and luminol was oxidized to the luminol radical anion (Zhang et al., 2012). Subsequently, luminol radical anions reacted with ROS to produce an ECL signal. CeO_2 could catalyze the oxidation–reduction reaction between luminol and H_2O_2 to form excited-state 3-aminophthalate anions, which emits light on relaxation to the ground state (Equation 3) (Zhang et al., 2012). Therefore, an ECL sensor for the cholesterol detection could be established by combining with these two reactions and quantifying the concentration of cholesterol.

3.3. Electrochemical and ECL behaviors of as-synthesized nanocomposites

The EIS is a useful tool for investigating the interfacial changes of an electrode, which normally includes a semicircular part and a linear part, and the semicircle diameter at higher frequencies corresponds to the electron-transfer resistance (Hu et al., 2012). Fig. 3A presented the impedance spectrum of each electrode modified stage. Compared with the CHIT/CeO_2/GCE (curve a), the Nyquist semicircle of CHIT/CeO_2-GR/GCE (curve b) and CHIT/CeO_2-NG/GCE (curve c) in 5.0 mM $K_3Fe(CN)_6/K_4Fe(CN)_6$ (1:1) decreased, indicating that graphene-based materials had the excellent conductivity while nitrogen-doping could further enhance the electron transfer (Jiang et al., 2015a). When the ChOx was immobilized onto the electrode, the Nyquist semicircle increased (curve d) due to hindrance caused by non-conductive ChOx (Zhang et al., 2012),[32] implying that the ChOx was successfully absorbed on the surface of the CeO_2-NG nanocomposites.

To explore the electrocatalytic activity of CeO_2-NG nanocomposites, a control experiment of different modified electrodes in the presence of the same H_2O_2 concentration (10 μM) was performed to record the ECL responses. The ECL behaviors of CHIT/bare/GCE, CHIT/CeO_2/GCE, CHIT/CeO_2-GR/GCE and CHIT/CeO_2-NG/GCE were investigated in 0.1 M PBS (pH 7.4) containing 0.1 mM luminol and 10 μM H_2O_2 (Fig 3C). It was noteworthy that the ECL emissions of CHIT/CeO_2-NG/GCE (curve d) were 3.33-fold enhanced compared with CHIT/CeO_2/GCE (curve b) in the presence of 10 μM H_2O_2. And it can be observed that the ECL onset potential of the CHIT/CeO_2-NG/GCE was 72 mV more positive

than that of CHIT/CeO_2/GCE, indicating that NG could decrease the potential barriers of the ECL reaction obviously (Du et al., 2015), which was consistent with the corresponding CVs (inset of Fig 3D). Besides, it should be highlighted that the ECL intensity from CHIT/CeO_2-NG/GCE was about 1.89-fold higher than that observed from CHIT/CeO_2-GR/GCE, which could be attributed to the introduction of nitrogen in graphene that provided a pair of electrons for conjugation with the π–conjugated rings, bringing electron donor properties to graphene and improve the electrochemical performances of NG (Du et al., 2015). All these results implied the ECL activity of CHIT/CeO_2-NG/GCE outperformed that of CHIT/CeO_2/GCE and it's expected that the biosensor based on CHIT/CeO_2-NG/GCE would possess excellent performances in applications.

3.4. Optimization of analytical conditions

To optimize the performances of the prepared ECL biosensor, the effect of the concentration of luminol on the ECL intensity was examined. The result showed that the ECL intensity increased with the increase of luminol concentration and reached a plateau when the concentration increased to 0.25 mM (Fig. 4A). Thus, considering the ECL intensity and the consumption of reagents, 0.20 mM was chosen as the optimal concentration of luminol in this work. In addition, the effect of the solution pH value from 5.0 to 9.0 on the performance of ECL biosensor was investigated. From Fig. 4B, the ECL intensity increased with increasing pH and the strongest ECL intensity was obtained at pH 7.4, indicating that the biosensor was more active at this pH and the immobilized ChOx kept its natural structure and did not denature (Cao et al., 2013).

Thus, pH 7.4 was selected through the whole experiment.

3.5. The quantificational detection of cholesterol

In order to evaluate the analytical application of the ECL emission of CHIT/CeO_2-NG/GCE and CHIT/CeO_2-GR/GCE, the developed biosensors were applied in the detection of cholesterol. Fig. 5A and Fig. 5C revealed the effect of various concentration of cholesterol on the ECL intensity of luminol solution on ChOx/CHIT/CeO_2-NG and ChOx/CHIT/CeO_2-GR modified electrodes, and the ECL intensity increased linearly with the increase of cholesterol concentration (Fig. 5B and Fig. 5D). Above all, the ChOx/CHIT/CeO_2-NG/GCE possessed a wider linear range (4 μM~5 mM) and lower detection limit (1.33 μM) (signal/noise [S/N]=3), while ChOx/CHIT/CeO_2-GR/GCE was in the linear range from 20 μM to 1.3 mM with the detection limit of 6.67 μM, which was compared with previous reports (Table S1). These results might be attributed to the introduction of nitrogen in graphene provided the ChOx with more accessible microenvironment which enlarge the sensitivity of the ECL sensitive detection.

3.6. The reproducibility and stability of the biosensor

In order to evaluate the repeatability of the ChOx/CHIT/CeO_2-NG biosensor, the relative ECL intensity of the biosensor was recorded under continuously cyclic potential scanning for 16 cycles in PBS containing 0.2 mM luminol and 0.1 mM cholesterol at the scan rate of 100 mV/s (Fig. 3B). No obvious change was observed when the ECL emission was repeated under continuous cyclic scans, suggesting that the constructed ECL detection method exhibited good stability for the cholesterol

determination. The relative standard deviation (RSD) for repetitive measurements (n= 9) of the biosensor response to 0.1 mM cholesterol (Fig. 3B) was 4.6%. The reproducibility of the biosensor was performed by 5 assaying electrodes prepared under the same conditions. The relative standard deviation (RSD) was 5.5% in the presence of 0.1 mM cholesterol solution.

3.7. Real sample analysis

The analytical application of the bienzymatic cholesterol sensor was evaluated by detecting cholesterol in human serum samples and commercial milk powder. The milk powder was pretreated by saponification and solvent extraction (Daneshfar et al., 2009). The milk powder and serum samples were diluted in such a way that, the cholesterol concentration should be between the detecting range of the above mentioned method. Three different concentrations of cholesterol were added into human serum and the milk powder samples, respectively, according to the standard addition method. Table S2 listed the recovery of six samples of different cholesterol concentrations. The recovery rate was from 97.0% and 112.5%. The satisfying results demonstrated that the biosensor had a great potential for practical application.

4. Conclusions

In summary, a one-step heat-treatment strategy was developed to synthesize CeO_2-NG nanocomposites absence of precursor, which exhibited improved electrocatalytic activity to luminol and generated an enhanced ECL emission in the neutral condition compared with CeO_2 NCs. The as-synthesized CeO_2-NG nanocomposites were further employed as matrices to immobilize ChOx for amplify

the ECL of luminol and a cholesterol biosensor was successfully constructed. Besides, a comparison of the electrochemical and ECL behavior between CeO_2-NG nanocomposites and pristine CeO_2 NCs was researched in luminol solution. The results demonstrated that CeO_2-NG nanocomposites exhibited more outstanding performances in terms of physical and chemical properties and catalytic activities than pristine CeO_2 NCs. The present work would be potentially meaningful for understanding the role of NG in electrochemistry and provide a promising approach to develop efficient biosensors in clinical application.

Acknowledgments

The present work was supported by the National Natural Science Foundation of China (Nos. 21175061, 21375050 and 21405063), a Project Funded by the Priority Academic Program Development of Jiangsu Higher Education Institutions (No. PAPD-2014-37), Qing Lan Project and Key Laboratory of Modern Agriculture Equipment and Technology (No. NZ201109).

References

Bai, S., Xiong, Y.J., 2015. Chem. Commun. 51, 10261–10271.

Ballesta-Claver, J., Ametis-Cabello, J., Morales-Sanfrutos, J., Megı´a-Ferna´ndez, A., Valencia-Miro´n, M.C., Santoyo-Gon-za´lez, F., Capita´n-Vallvey, L.F., 2012. Anal Chim Acta 754, 91–98.

Cao, S.R., Zhang, L., Chai, Y.Q., Yuan, R., 2013. Biosens. Bioelectron. 42, 532–538.

Chen, S.L., Luo, L.F., Jiang, Z.Q., Huang, W.X., 2015. ACS Catal. 5, 1653–1662.

Chu, Y.Y., Cao, J., Dai, Z., Tan, X.Y., 2014. J. Mater. Chem. A 2, 4038–4044.

Daneshfar, A., Khezeli, T., Lotfi, H.J., 2009. J. Chromatogr. B 877, 456–460.

Du, X.J., Jiang, D., Liu, Q., Qian, J., Mao, H.P., Wang, K., 2015. Talanta 132, 146–149.

Du, X.J., Zhang, D.S., Shi, L.Y., Gao, R.H., Zhang, J.P., 2012. J. Phys. Chem. C 116, 10009–10016.

Gilje, S., Han, S., Wang, M.S., Wang, K.L., Kaner, R.B., 2007. Nano Lett. 7, 3394–3398.

Guo, S.J., Wen, D., Zhai, Y.M., Dong, S.J., Wang, E.K., 2010. ACS Nano 4, 3959–3968.

Hong, L., Liu, A.L., Li, G.W., Chen, W., Lin, X.H., 2013. Biosens. Bioelectron. 43, 1–5.

Hu, Y.W., Wang, K.K., Zhang, Q.X., Li, F.H., Wu, T.S., Niu, L., 2012. Biomaterials 33, 1097–1106.

Jha, S.K., Kumar, C.N., Raj, R.P., Jha, N.S., Mohan, S., 2014. Electrochim. Acta 120, 308–313.

Ji, Z.Y., Shen, X.P., Yang, J.L., Zhu, G.X., Chen, K.M., 2014. Appl. Catal., B 144, 454–461.

Jiang, D., Du, X.J., Liu, Q., Zhou, L., Qian, J., Wang, K., 2015a. ACS Appl. Mater. Interfaces 7, 3093–3100.

Jiang, D., Du, X.J., Liu, Q., Hao, N., Qian, J., Dai, L.M., Mao, H.P., Wang, K., 2015b. Chem. Commun. 51, 4451–4454.

Jiang, D., Liu, Q., Wang, K., Qian, J., Dong, X.Y., Yang, Z.T., Du, X.J., Qiu, B.J., 2014. Biosens. Bioelectron. 54, 273–278.

Jiang, L.H., Yao, M.G., Liu, B., Li, Q.J., Liu, R., Lv, H., Lu, S.C., Gong, C., Zou, B., Cui, T., Liu, B.B., 2012a. J. Phys. Chem. C 116, 11741–11745.

Jin, J.C., Xu, Z.Q., Dong, P., Lai, L., Lan, J.Y., Jiang, F.L., Liu, Y., 2015. Carbon 94, 129–141.

Liao, L., Mai, H.X., Yuan, Q., Lu, H.B., Li, J.C., Liu, C., Yan, C.H., Shen, Z.X., Yu, T., 2008. J. Phys. Chem. C 112, 9061–9065.

Liu, X., Swihart, M.T., 2014. Chem. Soc. Rev. 43, 3908–3920.

Manorama, S.V., Izu, N., Shin, W., Natsubara, I., Murayama, N., 2003. Sens. Actuators, B 89, 299–304.

Mayavan, S., Sim, J.B., Choi, S.M., 2012. Carbon 50, 5148–5155.

Mokkelbost, T., Kaus, I., Grande, T., Einarsrud, M.A., 2004. Chem. Mater. 16, 5489–5494.

Nørskov, J.K., Bligaard, T., Rossmeisl, J., Christensen, C.H., 2009. Nat. Chem. 1, 37–46.

Rao, C.N.R., Sood, A.K., Subrahmanyam, K.S., Govindaraj, A., 2009. Angew. Chem., Int. Ed. 48, 7752–7777.

Schwarz, J.A., Contescu, C., Contescu, A., 1995. Chem. Rev. 95, 477–451.

Shah, M.S.A.S., Park, A.R., Zhang, K., Park, J.H., Yoo, P.J., 2012. ACS Appl. Mater. Interfaces 4, 3893–3901.

Srivastava, M., Das, A.K., Khanra, P., Uddin, M.E., Kima, N.H., Lee, J.H., 2013. J.

Mater. Chem. A 1, 9792–9801.

Su, Q.M., Chang, L., Zhang, J., Du, G.H., Xu, B.S., 2013. J. Phys. Chem. C 117, 4292–4298.

Wang, H.B., Maiyalagan, T., Wang, X., 2012a. ACS Catal. 2, 781–794.

Wang, X., Li, X.Y., Liu, D.P., Song, S.Y., Zhang, H.J., 2012b. Chem. Commun. 48, 2885–2887.

Xu, L., Huang, W.Q., Wang, L.L., Huang, G.F., 2014. ACS Appl. Mater. Interfaces 6, 20350–20357.

Yang, Y., Tian, C.G., Sun, L., Lv, R.J., Zhou, W., Shi, K.Y., Kan, K., Wang, J.C., Fu, H.G., 2013. J. Mater. Chem. A 1, 12742–12749.

Zhang, H.R., Wu, M.S., Xu, J.J., Chen, H.Y., 2014. Anal. Chem. 86, 3834–3840.

Zhang, M.H., Yuan, R., Chai, Y.Q., Chen, S.H., Zhong, H.A., Wang, C., Cheng, Y.F., 2012. Biosens. Bioelectron. 32, 288–292.

Zhang, Z.L., Han, D., Wei, S.J., Zhang, Y.X., 2010. J. Catal. 276, 16–23.

Scheme 1

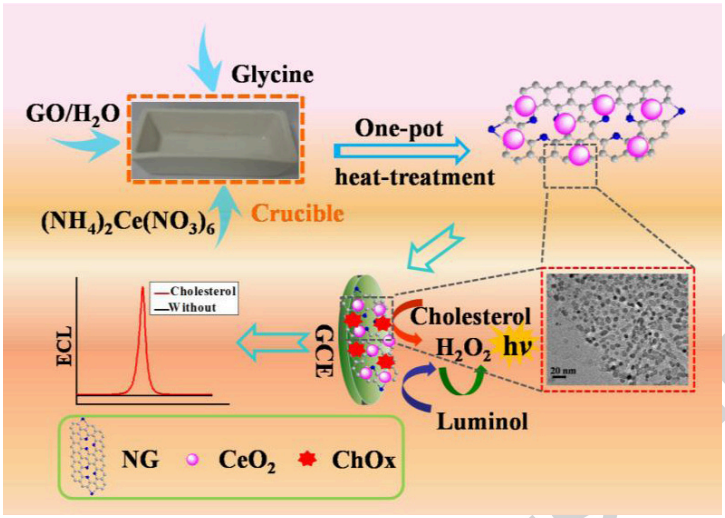

Scheme 1. The schematic presentation for one-pot heat-treatment synthesis of CeO_2-NG nanocomposites for the ECL cholesterol biosensor fabrication and its detecting mechanism.

Fig. 1

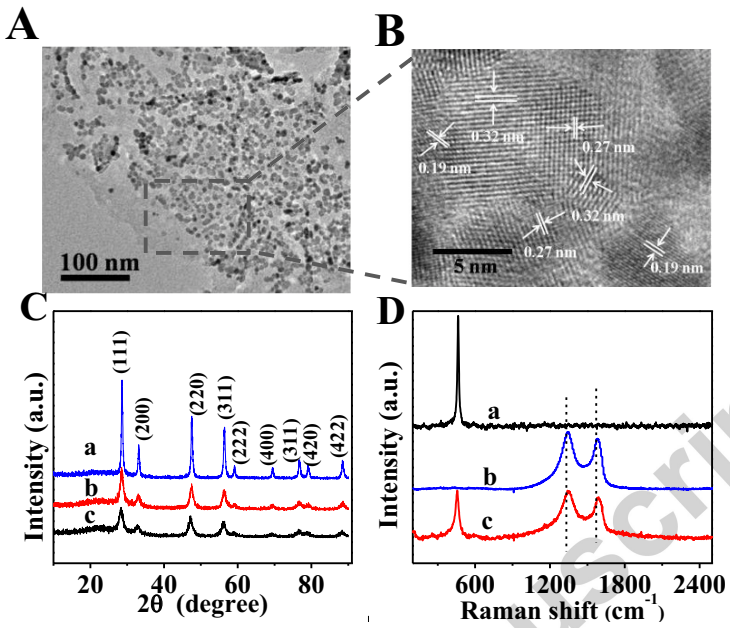

Fig. 1. TEM images of CeO_2-NG nanocomposites (A) and the HRTEM image of CeO_2-NG nanocomposites (B); (C) XRD pattern of CeO_2-NG nanocomposites (a) CeO_2-GR nanocomposites (b) and pristine CeO_2 NCs (c); (D) Raman spectra of pristine CeO_2 NCs (a) powdery NG (b) and CeO_2-NG nanocomposites (c).

Fig. 2

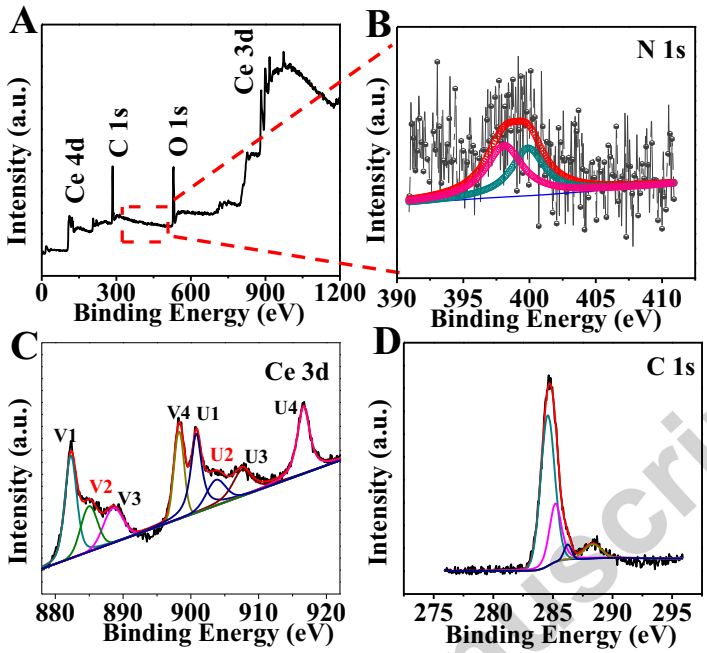

Fig. 2. (A) XPS survey scan of CeO_2-NG nanocomposites and the high-resolution XPS spectra of (B) N 1s, (C) Ce 3d, and (D) C 1s.

Fig. 3

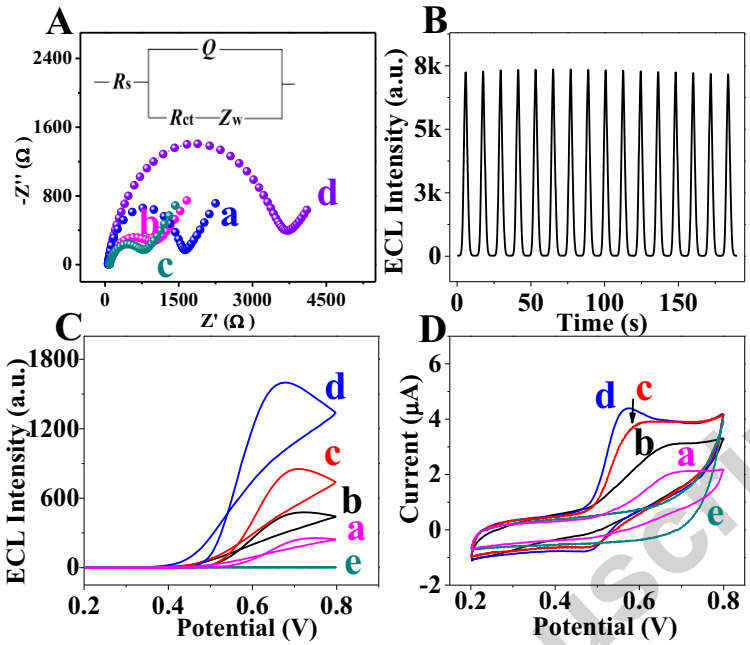

Fig. 3. (A) EIS of (a) CHIT/CeO_2/GCE, (b) CHIT/CeO_2-GR/GCE, (c) CHIT/CeO_2-NG/GCE and (d) ChOx/CHIT/CeO_2-NG/GCE in 5.0 mM $K_3[Fe(CN)_6]$/$K_4Fe(CN)_6$] (1:1). (B) The stability of the biosensor under consecutive cyclic potential scans for 16 cycles in 0.1 mM cholesterol solution. (C) ECL behaviors of (a) CHIT/bare/GCE, (b) CHIT/CeO_2/GCE, (c) CHIT/CeO_2-GR/GCE and (d) CHIT/CeO_2-NG/GCE in 0.10 M PBS (pH = 7.4) containing 0.2 mM luminol and 0.1 mM H_2O_2 and (e) CHIT/CeO_2-NG/GCE in 0.10 M pH 7.4 PBS without H_2O_2 and (D) the corresponding CVs.

Fig. 4

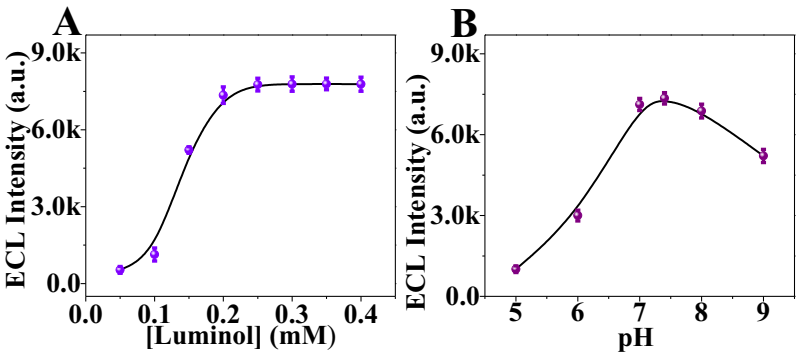

Fig. 4. (A) Effects of luminol concentration and (B) different pH on the ECL responses to cholesterol at ChOx/CHIT/CeO_2-NG/GCE in 0.1 M PBS.

Fig. 5¶

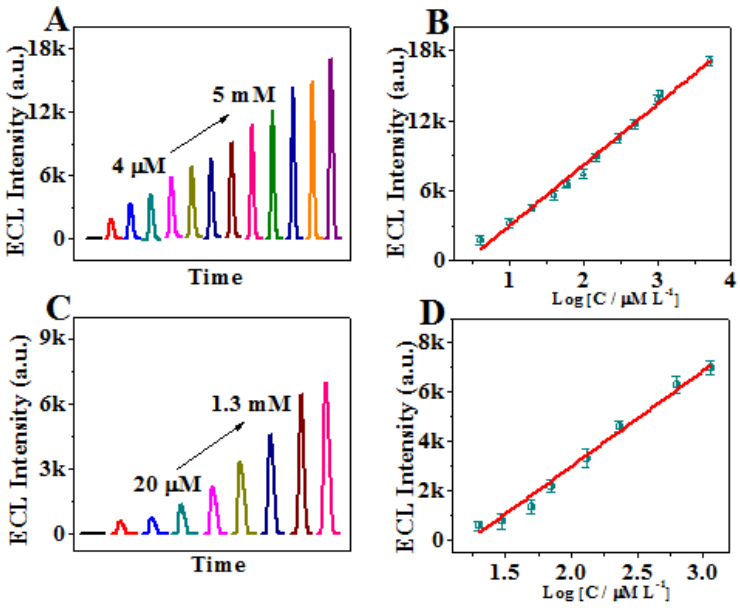

¶

Fig. 5. (A) ECL responses of ChOx/CHIT/CeO_2-NG/GCE from 4 μM to 5 mM cholesterol in 0.10 M PBS (pH 7.4) containing 0.2 mM luminol; (B) the linear relationship between the ECL signal intensity and the concentration of cholesterol. The ECL–time curves of (C) ChOx/CHIT/CeO_2-GR/GCE in 0.1 M PBS with different concentrations of cholesterol and the corresponding calibration curve for the cholesterol determination.¶

Page Break ¶

Highlights

► Nano-ensemble CeO_2 nanocrystallines-nitrogen-doped graphene (CeO_2-NG) was synthesized by a facile heat-treatment.

► CeO_2 NCs were well dispersed on the surface of NG sheets and the resultant CeO_2-NG nanocomposites were an excellent conducting material.

►The presence of the NG in CeO_2-NG nanocomposites could facilitate the electrochemical redox process of luminol compared with pristine CeO_2 NCs.

►The synthesized CeO_2-NG nanocomposites showed more enhanced the electrochemiluminescence emission in the neutral condition, as the matrix to immobilize enzyme for enzymatic sensing.